MITSUBISHI ELECTRIC RESEARCH LABORATORIES
https://www.merl.com

On-Orbit Additive Manufacturing of Parabolic Reflector via Solar Photopolymerization

Weiss, Avishai; Yerazunis, William S.; Radyjowski, Patryk; Cottrell, Richard

TR2019-125 October 31, 2019

Abstract

We consider an alternative solution for the conflicting requirements found in designing a spacecraft antennas, via on-orbit 3D printing. High gain and wide bandwidth depend upon large aperture, while economical orbital deployment dictates lightweight, sturdy, and small structures able to fit (or fold) inside the payload shroud of the launch vehicle. Finally, the antenna must function on orbit; a failed antenna deployment compromises the entire mission. Current solutions are to launch a final-shape unit (compromising on gain, and bandwidth), or to launch a folded antenna (compromising strength and reliability). An alternative solution is to 3D-print the antenna reflector on-orbit, using a photosensitive resin that polymerizes by crosslinking to a stable heat-resistant solid when exposed to UV. As the antenna is produced on orbit, in microgravity, it does not need to be any more robust than necessary to survive orbit correction maneuvers. Thus, it may be much thinner and lighter than a conventional antenna that must survive the stresses of launch and orbital insertion. After printing, the additional motors required for printing then become available for adjusting antenna focus, off-axis aiming, and beam pattern squint control, as well as aiming the antenna beam rapidly on orbit by using non-holonomic motions of the printed antenna against the main spacecraft bus.. As the antenna specifics are not determined until actual printing, it would be possible to pre-launch spare space vehicles and print the antenna with a specific (and possibly asymmetric) beam pattern on demand. To verify the feasibility of free-form 3D printing such structures with adequate shape control and surface smoothness to be used as spacecraft antennas, we built such a head-and-ram free-form 3D printer extruding several candidate resins. While bathing the printer in UV, and using an early candidate low-volatility resin, we successfully freeform-printed in air and earth gravity a 165mm (6.5") parabolic antenna with an f/1 focal ratio and a measured gain of 23.5 dB (vs a dipole) in the Ku band (13.5 GHz) with a simple dipole feed. Further resin candidates improved the strength-to-weight ratio by producing a desirable structural foam when extruded under vacuum of 25 millibar

International Astronautical Congress (IAC)

Mitsubishi Electric Research Laboratories, Inc.
201 Broadway, Cambridge, Massachusetts 02139

70th International Astronautical Congress (IAC), Washington D.C., United States, 21-25 October 2019.

IAC–19–C2.IP.2.x51358

On-Orbit Additive Manufacturing of Parabolic Reflectors via Solar Photopolymerization

William Yerazunis*, **Avishai Weiss***
Mitsubishi Electric Research Laboratories, USA, {yerazunis,weiss}@merl.com

Patryk Radyjowski[1]
The University of Texas at Austin, USA, patryk.radyjowski@gmail.com

Richard Cottrell
USA, cottrell@arczip.com

Abstract — We consider an alternative solution for the conflicting requirements found in designing a spacecraft antennas, via on-orbit 3D printing. High gain and wide bandwidth depend upon large aperture, while economical orbital deployment dictates lightweight, sturdy, and small structures able to fit (or fold) inside the payload shroud of the launch vehicle. Finally, the antenna must function on orbit; a failed antenna deployment compromises the entire mission. Current solutions are to launch a final-shape unit (compromising on gain, and bandwidth), or to launch a folded antenna (compromising strength and reliability). An alternative solution is to 3D-print the antenna reflector on-orbit, using a photosensitive resin that polymerizes by crosslinking to a stable heat-resistant solid when exposed to UV. As the antenna is produced on orbit, in microgravity, it does not need to be any more robust than necessary to survive orbit correction maneuvers. Thus, it may be much thinner and lighter than a conventional antenna that must survive the stresses of launch and orbital insertion. After printing, the additional motors required for printing then become available for adjusting antenna focus, off-axis aiming, and beam pattern squint control, as well as aiming the antenna beam rapidly on orbit by using non-holonomic motions of the printed antenna against the main spacecraft bus.. As the antenna specifics are not determined until actual printing, it would be possible to pre-launch spare space vehicles and print the antenna with a specific (and possibly asymmetric) beam pattern on demand. To verify the feasibility of free-form 3D printing such structures with adequate shape control and surface smoothness to be used as spacecraft antennas, we built such a head-and-ram free-form 3D printer extruding several candidate resins. While bathing the printer in UV, and using an early candidate low-volatility resin, we successfully freeform-printed in air and earth gravity a 165mm (6.5") parabolic antenna with an ∼f/1 focal ratio and a measured gain of 23.5 dB (vs a dipole) in the Ku band (13.5 GHz) with a simple dipole feed. Further resin candidates improved the strength-to-weight ratio by producing a desirable structural foam when extruded under vacuum of ∼25 millibar.

Nomenclature

3D freeform printing – 3D printing with only a minimal (if any) supporting substrate; layers may or may not be parallel or even continuous, unlike typical "by the slice" 3D printing of increasing Z-level cross-sections, starting from a flat and supporting substrate.

Oligomer – a partially polymerized resin. Unlike monomers that are composed of single unit-cell molecules, oligomers are chains of tens to tens of thousands of the unit cells. Such large molecules produce a liquid that is far more viscous and with a far lower vapor pressure than the original single unit-cell molecules of the monomer. Oligomers usually contain a number of available chemical bondsites (functional groups) and can be further polymerized.

Photoinitiator – a chemical that absorbs photons (usually deep blue or UV) and splits, producing free radicals and molecules that trigger polymerization of a monomer or oligomer. Photoinitiators can be catalytic or consumable. Typically 1 to 3 percent of an oligomer-based ready-to-print resin is photoinitiator.

Thermal polymerization – non-photoinitiated polymerization events. These are caused by the thermodynamically-rare event of a high energy oligomer molecule bonding to another molecule without the assistance of a photoinitiator or catalyst.

Inhibitor – the reverse of a photoinitiator. Typically these molecules scavenge free radicals, thereby preventing polymerization of the feedstock mix. To trigger polymeriation, enough UV is supplied to "burn through" the scavenging inhibitor molecules capacity and trigger bulk polymerization. Inhibitors also prevent thermal polymerization.

*Corresponding Authors.

[1]Patryk repeatedly interned and consulted with MERL during the development of this work.

Polymer – the fully polymerized resin. Linear resins are composed of long unbranching chains, usually remain meltable at some elevated temperatures (thermoplastic), and are formed by polymerizing monomers or oligomers with one functional group. Crosslinked resins, often called thermosetting resins for historical reasons, are formed from monomers or oligomers with two or more functional groups and generally can no longer be melted; at high temperatures ($> 300°$C) they slowly decompose into their component elements.

Plasticizer – a bulky molecule added to the feedstock that does not participate in the polymerization reaction. Instead, it separates strands of the polymer chains, providing room for the polymer chains to flex on the molecular scale without breaking. Addition of plasticizer prevents stress concentrations, cracking, and improves overall structural properties.

1. Introduction

Current satellite antennas are either deployed to orbit at full size, or are spring/motor actuated to unfold once in orbit. Full-size antennas take a lot of space, while unfolding antennas are mechanically complicated and prone to failure. Both antenna types must be made strong enough to withstand launch (5-10 G linear acceleration, and up to 50 G of broadband vibration [1]).

Because of their physical dimensions and stowage limitations, small satellites (SmallSats) do not currently have the ability to deploy large high-gain antennas. High gain antennas are especially useful on SmallSats due to the low transmitter power availability. However, with the advent of new launch opportunities, proposals for satellite constellations numbering in the thousands, and decreasing size and power consumption of on-board electronics, SmallSats are becoming commonplace. With their new popularity, increasing attention is now being paid to overcoming the aforementioned limits in communication ability. CubeSats, weighing between 1 and 10 kg, are particularly en vogue. In recent years a number of innovative solutions for CubeSats have been proposed, as discussed by Rahmat-Samii et al. [2] and references therein.

Briefly, highlights include inflatable antennas [3, 4] that have a high ratio of stowed volume to final deployed diameter but lack the surface quality for frequencies above X-band. Deployable reflectarrays flown in 2018 on MarCO (Mars Cube One) CubeSat mission to Mars [5] are lightweight and inexpensive, but the gain is limited based on how many panels can be folded into the CubeSat and also operate in X-band. Higher frequency Ka band deployable parabolic reflector meshes are described by Chahat et al. [6], but are mechanically complicated and require 1.5U of stowed volume for a $1m^2$ aperture. See Figure 2 in [6] for a comparison of patch, reflectarray, deployable mesh, and inflatable antennas.

The solution proposed in this paper doesn't launch with any high-gain antenna, folded, deflated, or otherwise compromised to fit into the spacecraft envelope or payload shroud. The antenna material experiences the launch as a tank of liquid resin 3D printer feedstock, so it's small, conformable, and totally immune to vibration and shocks. The antenna is 3D-printed after the satellite is in orbit and all future stresses are low. The antenna shape (which controls beam shape and focus) is not constrained to fit inside the launch vehicle, doesn't need to be foldable, and does not need strong support structures so it may actually be lower-mass than other alternatives. The motors used during on-orbit 3D printing can continue to be used after fabrication to aim the antenna beam rapidly during the mission by using non-holonomic motions of the printed antenna's inertial mass against the main spacecraft bus. As the shortest usable wavelength of the reflector is inversely proportional to the surface roughness, the submillimeter-level smoothness of a 3D printed reflector allows much higher frequency operation. We can further lighten the system by using the Sun as a UV source to supply the polymerization energy required to cure the resin.

2. Concept and Initial Feasibility

Thus, we define our minimum feasible system to demonstrate feasibility of a specialized on-orbit antenna 3D-printer:

- printer operates in the orbital space environment,
- can print and deploy a working communication antenna in a desired communication band,
- operated with the limited power available to a small satellite,
- the resulting structure can retain integrity when in the radiation, vacuum, and temperature extremes environment of space.

As this is a freeform 3D print, we start with a minimal hub mounted on the spin motor, and work outward from that. Figure 1 shows the progression of an antenna paraboloid being printed on a 3U or 6U

cubesat. The extruder nozzle is the small rectangle on the lower left of the spacecraft bus.

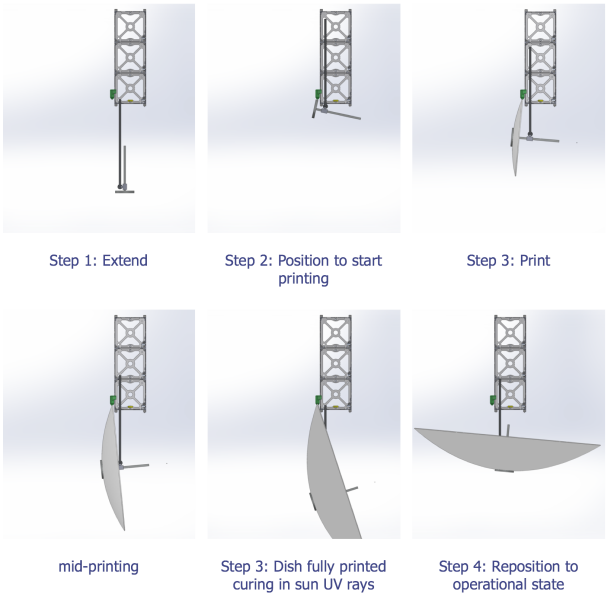

Fig. 1: Steps in the freeform 3D printing of a parabolic antenna. Full video available at `https://youtu.be/MmencoxoSwc`

2.1 Comparison - Mass at Launch

To be actually useful, in-space fabrication must not just be technically feasible, it must also be economically feasible. In the case of small comsats, that means it has to work well enough and be lower mass at launch than the current technology.

For a first-order test case, consider the Cassini probe's large fixed parabolic high gain antenna (a large antenna, but one with abundant publicly available information), Cassini's dish was 4 meters in diameter, and weighed 105 Kg [7, 8]. The dish was driven at three wavelengths - 14 cm (S band), 4 cm (X band, about 6 GHz), and 1 cm (Ka band, about 25 GHz), meanings the surface geometric accuracy had to be within 3.5cm, 1cm and 0.25cm respectively.

An equivalent 3D printed dish, 4 meters in diameter, 50 mm thick, would have a volume of 0.64 m^3, and if constructed monolithically from commercial two-part urethane foam (32 Kg / m^3) , would weigh only 20 Kg.

However, we must also account for the 3D freeform printer needed to construct the antenna disk on orbit. Given our experience gained actually constructing 3D freeform printers (see below text and figures), we estimate that the empty tank with inside bladder, pressurizer, metering valves, nozzle, sunlight shutter, extendable ram, tilt and spin motors, metallizer, and electronics would weigh on the order of 25 to 30 Kg, with a volume on the order of 40 to 50 liters. This translates to a 2X saving in launch mass, a considerably smaller payload shroud, and adds the benefit of non-holonomic spacecraft attitude control without propellant use.

Admittedly, freeform 3D printed antennas do add several points of failure, so the mass saving needs to be balanced against other issues. In situations where only a single space probe is launched (and the probe is very high value, e.g. Cassini at 3+ billion dollars total) then on-orbit printing may not be worth the risk unless the antenna gain required for the mission is so high that no other technology can accommodate the aperture requirement. But if one is going to launch on the order of a hundred near-identical smallsats in one launch event (with the anticipation that 10% of them fail to correctly print their antennas), but the lower mass and payload shroud volume savings allowed an additional twenty smallsats to be launched (20% increase in satellite number), overall the printed antenna becomes a statistical winning bet. The freeform 3D printed antenna may also have much lower initial cost compared to an intricate mechanical folding antenna of similar aperture and surface figure quality.

2.2 The Extra Motors Are Actually Useful

The full 3D manufacturing capability requires at least 3 positioning actuators. It is possible to reduce the actuation requirement to 2 motors for a limited subset of simple geometries (for example, having the spin motor also operate the extension ram screw) or even a single motor (directly driving the spin motor, geared down for the ram screw, and having tilt angle generated passively by a cam riding on the ram extension. Furthermore it should be noted that the microgravity environment enables utilization of much smaller and lighter motors as compared to ground-based units, and that during the high G-loads at launch the motors and motor support structures are only carrying their own mass, not the mass of the entire antenna dish.

One might continue to consider that the extrusion ram, ram motor, spin motor, and off-angle motor are wasted mass once the antenna element has been completed, but they maintain usefulness for the duration of the mission. Extending / retracting the ram will change the system RF focus and spot size. The off-angle motor, initially used to sculpt the paraboloid's

curve, later allows off-axis feedpoints or slewing the beam without using propellant. The spin motor can likewise slew the spacecraft (using the mass of the antenna as a reaction wheel), or, in the case of an intentionally-asymmetric reflector, can rotate the beam pattern to match the on-ground footprint of the desired service area.

Because the constructed element is truly freeform, arbitrary antenna patterns can be constructed; paraboloids are merely a good (and broadband) example of the antenna element. Diffractive elements are as easy to construct as reflective elements and may have a better launch mass to gain ratio, and require no metalization. The same constructed element may act as a wide-pattern antenna on S-band and a narrow pencil-beam at 15 GHz - and with different beam axes, by proper design.

Because vacuum deposition of metal onto plastic is an established and heavily commercialized technology, we will not further concern ourselves with it in this proof of concept.

3. Experimental Hardware

3.1 Test Extruder

In order to test the freeform 3D printability required for on-orbit fabrication of antenna structures, we designed and constructed an Arduino-controlled freeform extruder that could fit into our 500mm spherical vacuum chamber. The CAD model of the extruder is shown in Figure 2 and the actual build is shown in Figure 3.

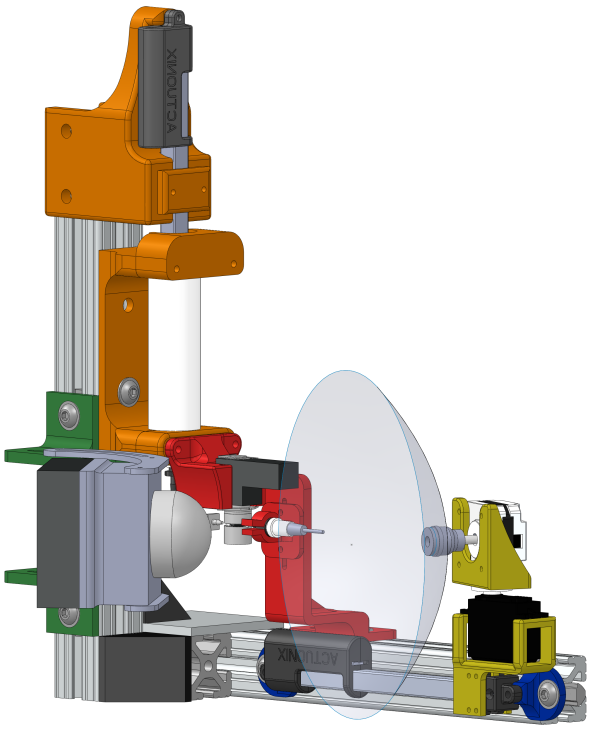

Fig. 2: Extruder CAD model.

Unlike a standard consumer 3D printer with three orthogonal linear translating axes, the test extruder is designed to adhere as closely as possible to the Cubesat-compatible design shown in Figure 1, including the multi-purpose motors. The positioning system consist of a single linear ram, also used to adjust beam focus on orbit, and two rotary axes, (one later to become the the RF feed off-axis angle (squint) control; the other motor rotates the paraboloid relative to the cubesat for printing, and later would allow alignment of an ellipsoidal or other asymmetric beam pattern onto ground sites without altering beam polarization.

A separate resin delivery system uses second linear ram to drive a piston in a large reservoir of viscous resin maintaining an elevated pressure relative to the local environment (room air or vacuum) via a differential pressure sensor and a bang-bang controller. Actual resin deposition is controlled by an electromagnetic pinch valve which pinches the silicone feed tube shut. The combination of tank pressure and rapid cyclic opening of pinched tube allow the desired flow rate to exit via a pliable 1.7mm ID nozzle. The high viscosity of the resin creates a sufficient retarding force to prevent rapid depressurization at a short timescale the valve remains open. The immediate exposure to high dose of UV radiation causes rapid polymerization with minimal influence of vacuum environment. The extrusion speed, resin composition and UV power are key factors necessary to fine-tuning the polymerization response upon exiting the nozzle. It was possible to achieve a repetitive, successful attachment onto the edge of the partially fabricated antenna reflector, where the UV light polymerizes it within a few seconds into rigid antenna material.

The entire system is controlled by two Arduino-based control systems; one outside the vacuum chamber operating a display and an operator manual controls, the other inside the chamber, directly controlling the motion and resin deposition systems apparatus. The communication between microcontrollers is based on a bidirectional serial optical link through the clear vacuum chamber wall. Power at 24VDC is supplied into the vacuum chamber via two copper foil lead-throughs laid across the silicone chamber gasket and heavily greased. Vacuum is produced by a Har-

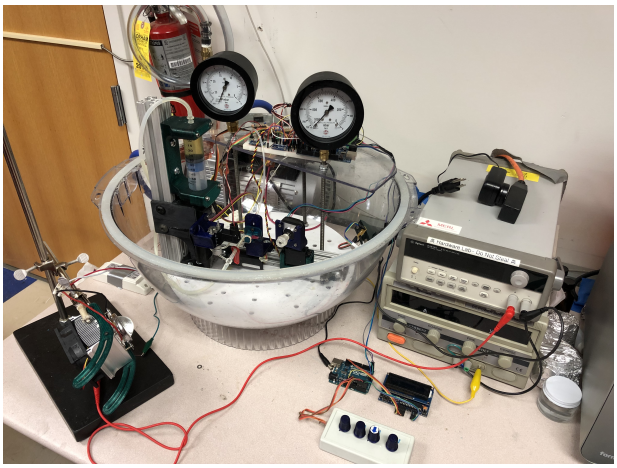

Fig. 3: Actual 3D freeform extruder system, in lower half of vacuum chamber.

bor Freight two-stage piston vacuum pump, and the pump exhaust is fed directly to a rooftop exhaust equipped with a large (500 watt) fan producing negative pressure on the entire in-building air path, to assure experimenter safety in case of unexpected outgassing of any unanticipated by-products, as well as safe extraction of any oil fog from the vacuum pump itself.

After loading the mixed and degassed feedstock resin into the resin reservoir, the system is switched to a semi-autonomous mode. The internal Arduino is then in control; the outside Arduino can read reservoir pressure, paraboloid rotation rate, feed-angle (squint) rate, ram rate, and pinch valve duty cycle, and can write the setpoints for those parameters, while the inside Arduino performs the actual controlling, stepping, and PWMing to achieve those setpoints.

We have used this system, with minor alterations, to produce testable 3D freeform antenna structures in both air and low quality (∼5 kPa) vacuum.

4. Photopolymerizable Resins

There are several constraints on the resin mix. Obviously, it must polymerize on exposure to bright light; chemical kinetics and ease-of-use criteria usually drive preference to intense exposure to deep blue and ultraviolet light (< 405 nm wavelength). Equally important but less obviously, it must *not* polymerize under any other condition, including heat, cold, shock, low level ionizing radiation, residual catalysts from plastic tubing or fittings, or surface ion contamination from metal parts in the extruder fluid handling path.

Silicone Tubing	safe
Latex Tubing	clogs
Nylon Barb Fittings	clogs
Polypropylene Barb Fittings	safe
Polycarbonate Barb Fittings	safe
Polyethylene Barb Fittings	clogs
Polyethylene Syringes	safe
Stainless Steel 304	safe for days, not weeks
Teflon-coated Stainless	safe
Neoprene Rubber (used in syringes)	safe

Table 1: Summary of the experimental determination of material compatibility for our custom resin.

It is critical to protect the uncured resin in the storage and delivery system from UV exposure. The summary of compatible material choices is presented in Table 1. None of the tested materials, except the stainless steel, block UV radiation, therefore a metal foil shielding has been used whenever UV source has been in operation.

4.1 Consumer Resins

For initial feasibilty testing, we started with an inexpensive consumer-grade premixed feedstock resin: FormLabs Clear, Version 4. This resin has a moderate vapor pressure due to dissolved oxygen, making it foam wildly at low (< 50) millibars pressure, but for testing overall concepts in air and 1G local gravity, it provided an easy starting point that could be test-verified in our Formlabs printer as to UV sensitivity and physical properties such as strength and yield point, verifying that our extrusion and polymerization process were within reasonable bounds for at least one resin.

We had several atmospheric-pressure successes using this resin to free-form fabricate test articles for RF gain measurement (results below).

However, when degassed to a post-foaming stable pressure < 20 millibars, FormLabs Clear V4 becomes extremely susceptible to thermal polymerization and becomes highly photosensitive to extremely rapid photopolymerization, hardening before the resin could bridge the 1-2mm gap between the extruder nozzle and the initial spindle base. We surmise that this is due to the degassing removing dissolved oxygen, and this lack of oxygen blocking the ther-

mal inhibitors utilized in this consumer-grade product. Molecular oxygen, usually present through diffusion from earth atmosphere, is a necessary adjunct for many polymerization inhibitors to function. The exposure to pressures under 20 millibars removes this dissolved oxygen, hence suppressing inhibitor action and causing the hyperactivity of polymerization initiators.

As the actual formulation of the FormLabs resin is proprietary it is not possible to further investigate this material. We then proceeded to research our own formulations of extruder feedstock.

4.2 Custom Resins

Our current research resin is composed of a low-volatility aliphatic urethane acrylate oligomer blend, a photoinitiator, an inhibitor, and a low volatility polyphenol ether oil to act as a plasticizer and to decrease the viscosity of the otherwise-greaselike oligomer. The polyphenyl ether oil and the crosslinked polymers formed from the aliphatic urethane acrylates are chemically compatible and form stable homogenous solid mixtures.

More specifically, we have converged toward an oligomer-only feedstock composed by weight of 10% Sartomer CN9013 oligomer, 10% CN991 oligomer, 40% CN968 oligomer (all three are aliphatic urethane acrylate oligomers), and 40% Santovac 9 vacuum oil, giving a resin base feedstock with a viscosity of about 2000 cps. To this feedstock we then add sensitizers and stabilizers, typically 1% (by weight over the feedstock) BAPO (bis-acylphosphine oxide) as a photoinitiator, and 3% of 4-MP (4-methoxyphenol) as a thermal polymerization inhibitor. Additionally, we add a very small amount (0.37% by weight) of BYK-088 (a commercially available long-chain alkane mix) as an antifoaming agent to assist in degassing.

The justification for the large fraction (40%) of CN968 is that the CN968 oligomeer is formulated with six functional groups (bondable crosslinking sites), which produce a strong and warp-resistant polymer matrix; this oligomer has an unreacted base viscosity of about 3500 cps (comparable to molasses on a cold day). The CN991 has two functional groups, and a base viscosity of 7000 cps, while the CN 9013 has nine functional groups and a viscosity of 180,000 cps (nearly solid). The Santovac 9 vacuum oil has a viscosity of just 190 cps (comparable to quality spar varnish) and makes the mixing and defoaming process much more tractable.

The final extruder feedstock mixture, including the oligomer mix, photoinitiator, inhibitor, and antifoamer is then degassed at 5 kPa and 60 degC in a vacuum oven for 15 minutes before loading into our extruder. We estimate that the ready-to-extrude material has a viscosity of roughly 2000 cps at room temperature.

To further reduce viscosity we tested a mix of CN968 60% (3500 cps) with Santovac 9 40% (190 cps) but found that toughness suffered; samples were brittle, rather than tough and strong; our qualitative observation is that too much crosslinking can be as bad as too little, even in the presence of large (40%) plasticizer fractions. Increasing the Santovac 9 fraction from 40% Santovac 9 to 60% Santovac 9 (with straight 40% CN968, no CN9013 or CN991) polymerized to samples with an oily surface as the Santovac 9 plasticizer was no longer fully contained in the polymer matrix.

5. Experiments in air

Many of our preliminary experiments have been performed at room temperature and pressure. This allows us to verify best case surface figure of a 3D freeform printed object, speed of printing, and any other factors, given that a hypothetical "perfect" vacuum-compatible extruder feedstock existed.

Given the constraints of our extruder (more specifically, that it had to fit inside a 1/2 meter spherical vacuum chamber) and the size of our resin reservoir, the largest possible paraboloid we can currently produce is ∼165 mm (6.5 inches) in diameter. We successfully and repeatably fabricated paraboloids of this diameter, typically with a nominal f/1 aperture ratio (that is, nominally a 160-170mm focal length). The process is partially automated; the software keeps the proper angle and ram offset correct so that the extrusion is an accurate paraboloid, closes the loop on the resin reservoir pressure, varies the spin rate to achieve constant rim linear speed, and maintains the desired resin flow rate via the pinch valve. The human operator supervises the printing process, modifying the setpoints for rotation speed, extruder pressure, pinch valve PWM duration, rotation rate, and ram extrusion rate, to correct for any variation in viscosity or polymerization time encountered.

Figure 4 shows the 3D freeform printer in action, printing a 160mm f/1 paraboloid using FormLabs Clear resin, at atmospheric pressure. The polymerization energy UV source is an LED array at the far left, outputting a nominal 405nm beam; at the ranges used, this UV source delivered ∼5 milliwatts / cm^2 (0.5 watts / m^2, so eye protection is

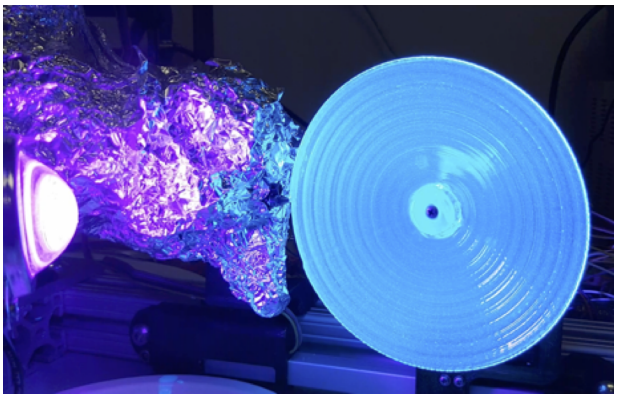

Fig. 4: Printing in air. The UV source is at the far left; the extruder is shielded with aluminium foil. The resin being printed is Form-Labs Clear, Version 4. Full video available at `https://youtu.be/XDsexqd30Gg`

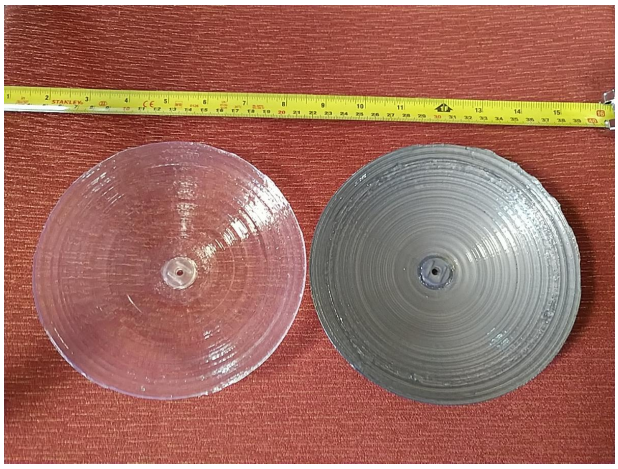

Fig. 5: A pair of ∼160mm f/1 paraboloid reflectors printed in air. The left paraboloid is left as-produced; the right paraboloid has been coated with a spray-on conductive coating for RF performance testing

mandatory) at the polymerization zone, as measured by a ThorLabs PM100A photometer with an S401C broadband bolometer sensor. As configured, polymerization took 1-3 seconds.

Figure 5 shows a pair of 160mm diameter by ∼1.75mm thick f/1 paraboloids fabricated at room conditions; both specimens are printed using Form-Labs V4 resin, where the gray one is additionally coated with a conductive coating (spray-on Super-Shield, from MG Chemicals) for RF testing. The coated paraboloid weighs 37.1 grams while the uncoated paraboloid weighs 34.0 grams. Note that in a real system, vacuum metallization with aluminium or gold would be greatly preferred over commercial spray-can metallization preparations.

5.1 RF characterization

Gain and sidelobe size is of paramount importance for any directional antenna, so we experimentally verified one of the produced test articles with an Agilent M5230A two-port network analyzer and a pair of self-made 22 mm dipole antennas with a nominal self-resonance at 12 GHz. Figure 6 shows the configuration of the test paraboloid, with the dipole and RF feedline.

Lacking an anechoic RF test chamber, we made approximate measurements in an open unobstructed lab area, alternating between bare dipoles (establishing a path loss baseline) and with one dipole equipped with the test paraboloid (the other dipole remained bare). We tested roughly every five degrees in azimuth, from -90 to +90 degrees, at 10, 13.5, and 20 GHz.

Figure 7 shows the actual mainlobe gains for 10 GHz to be about 21.5* dB, a gain of 23.5* dB at 13.5 GHz, and a gain of 15.5* dB at 20 GHz. Sidelobes were generally 12 dB below the mainlobe gain, and slightly asymmetric in ways we only partially understand.

As the feed was a simple unshielded dipole, these gain numbers are clearly suboptimal compared to a feedpoint that would actually be used in a proper CubeSat implementation. The unshielded dipole RF feed radiates in a equatorial torus pattern with nulls along the wire axis at the 12 GHz self-resonant freqency (other radiation patterns appear at other wavelengths) so in the best case, about 2/3 of the testing energy radiated from the dipole misses the paraboloid completely and contributes nothing to gain. Replacing the unshielded dipole feed with a directional (but still wideband) horn feed at the focal point should gain 4 to 5 dB with no other system changes. The seemingly-weak performance at 20 GHz is explainable by the primitive dipole feedpoint; for a constant length dipole, increasing the drive frequency past the resonant frequency causes the dipole's equatorial radiation lobe to become even less directional, putting more energy toward the near-polar axis. This cuts the available energy in the region that the paraboloid can capture and focus.

The surface roughness is probably not a limit-

*Note that in a prior version of this publication the gains were incorrectly reported. The gains have been updated.

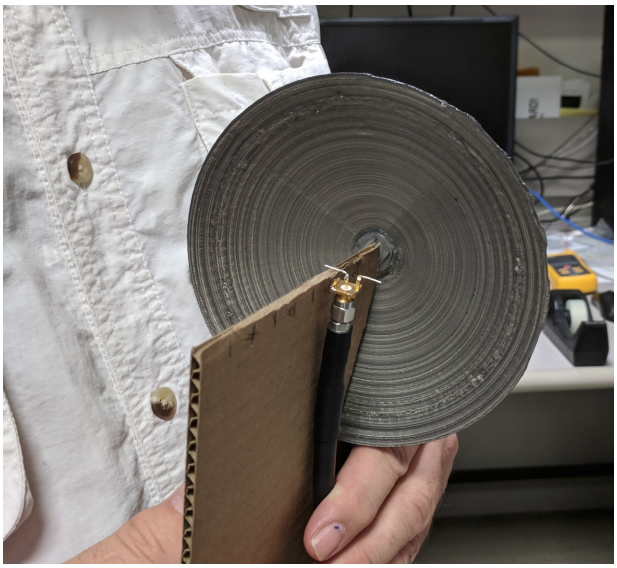

Fig. 6: The coated test paraboloids configured with a dipole for gain and focal length testing. The dipole is cut to 22mm tip-to-tip and therefore has a nominal resonance at ∼12 GHz

ing factor in beam quality. Measurement of a test paraboloid on the convex surface (the metallized surface) showed worst-case deviations on the order of ± 250 microns; assuming 250 microns as the surface deviation of a $\lambda/4$ diffraction limited reflector indicates the reflector surface quality is adequate to focus wavelengths as short as 1 mm (that is, ∼300 GHz). We cannot verify this as our test equipment cannot reach those frequencies so we emphasize that this is purely hypothesis.

6. Experiments in vacuum

As noted above, using a consumer grade resin while under vacuum did not produce satisfactory results due to outgassing, causing failure of the oxygen-dependent polymerization inhibitor due to very low oxygen concentrations. Switching to a custom low-volatility mixture (described above) allowed us to effectively print at far lower (but not proven at space environment) pressures, as shown by the printer during vacuum operation in Figure 8.

Figure 9 shows a pair of 60mm paraboloids printed in the above low-volatility resin. Approximately 40 mL of the low-volatility resin was given a final degassing at ∼5 kPa, then vacuum-loaded via siphon action into the extruder. A fresh hub was placed on the ram, and the first (transparent) 60mm paraboloid printed with the vacuum chamber open to room air.

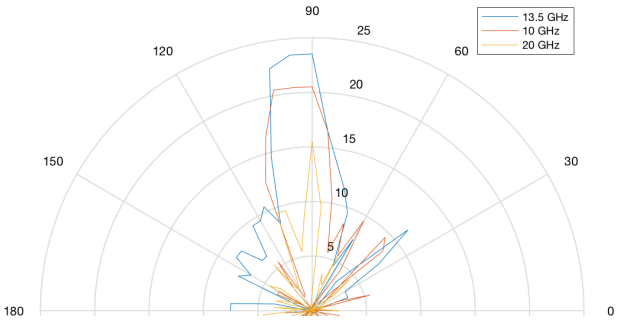

Fig. 7: Gain over a free-space dipole at 10 gHz, 13.5 gHz, and 20 gHz, all tested with the 22mm (12 GHz) dipole feed.

The result is the left (clear) paraboloid of Figure 9.

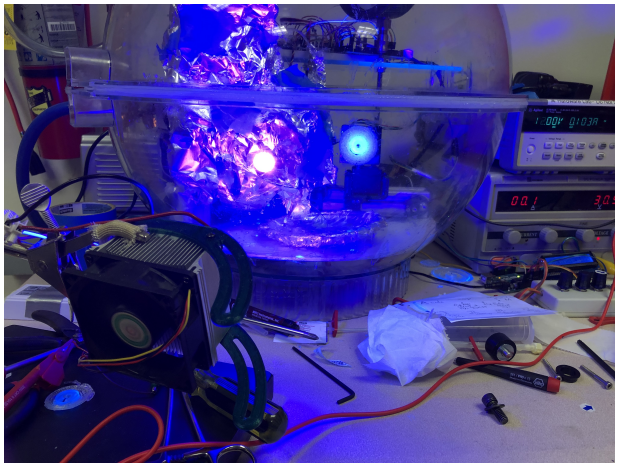

Fig. 8: 3D freeform printing in low quality vacuum. The pressure in the chamber is ∼5 kPa and slight foaming is occurring during the printing. Full video is available at `https://youtu.be/AtbX_LCb9IQ`

This first transparent printed paraboloid was replaced with a fresh hub, the ram and skew angle reset, and the vacuum chamber closed and evacuated down to 5 kPa; and some resin test-flowed. A thin line of extremely fine bubbles appeared in the short tube between the PWMed pinch valve and the nozzle, but we considered them insignificant at that time. We repressurized the vacuum chamber, shielded the extruder with aluminium foil, and pumped it back down to 5 kPa. We then proceeded to print the second 60mm paraboloid at an ambient pressure of about 5 kPa using the remaining resin load; this allows a directly comparable materials test.

The fine bubbles persisted, but only in the line downstream of the PWMed pinch valve; the bubbles

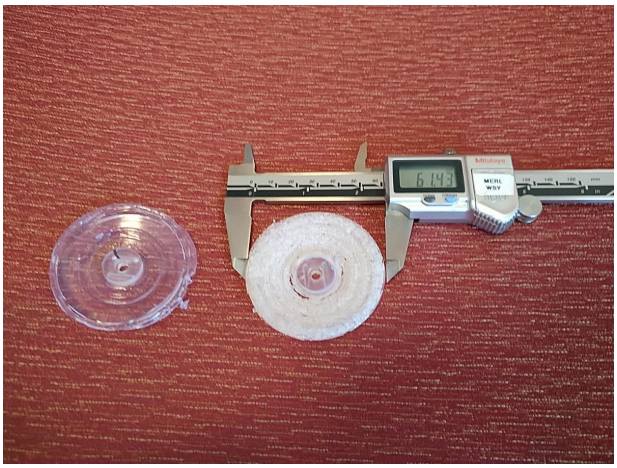

Fig. 9: Two 60mm test paraboloids. The left paraboloid was printed with our low-volatility resin at room temperature and pressure (20 degC and 100 kPa); the right paraboloid was printed a few minutes later from the same resin load but at about 5kPa pressure. Very mild foaming occurred in the vacuum-printed paraboloid but the surface roughness is quite acceptable.

did not interfere with the print. We terminated this second print due to exhaustion of the resin reservoir; interestingly as the reservoir emptied, the closed-loop pressure control ran out of authority, the delivery line pressure fell, and the pinch-valve PWM was set fully open. At this point the creation of the fine bubbles ceased and the final printed layer of the second (whitish) paraboloid were produced clear and bubble-free.

We found it interesting that the fine-grained foam produced a paraboloid with less mass and greater stiffness than the first (atmospheric pressure) paraboloid. This confirms that foaming is a valid optional method to further enhance the usefulness of this style of on-orbit fabrication.

In fact, it may be desirable to intentionally introduce controlled amounts of a foaming agent into the viscous resin, either premixed on the ground before launch or added during extrusion to further modify the properties of the polymerized material. As noted by Kizito et al. [9], sufficiently small gas bubbles (on the order of tens of microns across) embedded in a viscous liquid exposed to space-level vacuums do not expand without bound as the ideal gas law initially suggests, but are opposed by surface tension and reach an equilibrium size within a few seconds, at low but non-spacelike interior pressures (eg in silicone oil, for a 30 micron air bubble introduced at 50 KPa, the measured stable space-vacuum size is 185 microns at a calculated 0.21 KPa interior pressure).

7. Conclusions, Observations, and Future Work

The work documented above demonstrates proof of concept of some, but not all, of the technology required to implement on-orbit 3D freeform printing in the space environment.

7.1 3D Freeform Photopolymerization Printing

Given the results above, it is clear that the electromechanical and photopolymerization aspects of unsupported 3D freeform printing an antenna element such as a paraboloid or diffraction beamformer is reasonable and demonstrated.

7.2 Acceptable Quality of Surface Figure and RF Gain

Given the RF performance testing, it is clear that the RF performance of a 3D freeform printed antenna structure has adequate beamforming performance for microwave (∼10 to 13.5 GHz) communications use. Usefulness in a wider band is expected but not proven.

7.3 Vacuum-compatible Photopolymerizing Resins are Probably Feasible

Our results above show that while some consumer-grade resins are not compatible with printing in a space environment due to O_2 inhibition failure, premature polymerization, and photoinitiator boil-off, other known and commercially available photoinitiator and inhibitor families do not share this volatility and O_2 dependence, and may be sufficiently well behaved to not require further chemistry development but merely proper selection, purchase, and mixing with a blend of commercially available oligomers and plasticizers to yield an extruder feed suitable to the LEO environment.

7.4 On-orbit Metallization

Our results above omit in-vacuum metallization and merely use a spray-can of commercially conductive spray (MG Chemicals Super-Shield). Noting that the technology of vacuum metal deposition from a hot aluminium source is well known and used in many consumer food product wraps for UV blocking; in particular polyester films for snack food packagings are often vacuum metallized at massive consumer

scales, so we do not concern ourselves with this technology.

Therefore, we do not consider lack of demonstration of in-space metallization to be detrimental for the findings presented in this paper.

7.5 Space-worthiness and Orbital Debris

We have not examined the emanation of particulates during photoresin extrusion and curing. We do know that under some poorly characterized circumstances and blends, that the polymerizing resin may exothermically heat, bubble, and spatter before fully hardening. Any spattered particles will be in their own orbits and may contribute to LEO orbital debris; as they are sub-millimeter in size and entirely made of plastic they will be essentially untrackable on radar and may constitute an orbital collision hazard.

Therefore, until the magnitude of this threat can be determined, we caution that any in-space demonstration with photopolymerizing resins be carried out in orbits that, given the mass and drag cross section of small plastic fragments, any undesired fragments will reenter the atmosphere in a very short period, perhaps a week to a month, or alternatively, not initiating the 3D freeform printing until completing an orbital transfer burn that would cause any microparticles to exit the vicinity of Earth on a permanent basis.

References

[1] A. Harper, M. Ryschkewitsch, A. Obenschain, and R. Day, "General Environmental Verification Standard (GEVS) for GSFC Flight Programs and Projects," *NASA Goddard Space Flight Center, GSFC-STD-7000*, 2005.

[2] Y. Rahmat-Samii, V. Manohar, and J. M. Kovitz, "For satellites, think small, dream big: A review of recent antenna developments for cubesats." *IEEE Antennas and Propagation Magazine*, vol. 59, no. 2, pp. 22–30, 2017.

[3] A. Babuscia, B. Corbin, M. Knapp, R. Jensen-Clem, M. Van de Loo, and S. Seager, "Inflatable antenna for cubesats: Motivation for development and antenna design," *Acta Astronautica*, vol. 91, pp. 322–332, 2013.

[4] A. Babuscia, J. Sauder, A. Chandra, J. Thangavelautham, L. Feruglio, and N. Bienert, "Inflatable antenna for cubesat: A new spherical design for increased x-band gain," in *2017 IEEE Aerospace Conference*. IEEE, 2017, pp. 1–10.

[5] R. E. Hodges, N. Chahat, D. J. Hoppe, and J. D. Vacchione, "A Deployable High-Gain Antenna Bound for Mars: Developing a new folded-panel reflectarray for the first CubeSat mission to Mars." *IEEE Antennas and Propagation Magazine*, vol. 59, no. 2, pp. 39–49, 2017.

[6] N. Chahat, R. E. Hodges, J. Sauder, M. Thomson, E. Peral, and Y. Rahmat-Samii, "Cubesat deployable ka-band mesh reflector antenna development for earth science missions," *IEEE Transactions on Antennas and Propagation*, vol. 64, no. 6, pp. 2083–2093, 2016.

[7] J. Taylor, L. Sakamoto, and C.-J. Wong, "Cassini Orbiter/Huygens Probe Telecommunications," 2002. [Online]. Available: https://descanso.jpl.nasa.gov/DPSummary/Descanso3–Cassini2.pdf

[8] K. S. Smith and C. Y. Peng, "Air Mass Effects on the Cassini High Gain Antenna," vol. 3089, p. 319, 1997.

[9] J. Kizito, R. Balasubramaniam, H. Nahra, J. Agui, and D. Troung, "Vapor-gas bubble evolution and growth in extremely viscous fluids under vacuum," in *47th AIAA Aerospace Sciences Meeting including the New Horizons Forum and Aerospace Exposition*, 2009, p. 1147.